Measurement of J/ψ photoproduction at large momentum transfer at HERA

ZEUS Collaboration

ABSTRACT: The proton-dissociative diffractive photoproduction of J/ψ mesons has been studied in *ep* collisions with the ZEUS detector at HERA using an integrated luminosity of 112 pb^{-1}. The cross section is presented as a function of the photon-proton centre-of-mass energy and of the squared four-momentum transfer at the proton vertex. The results are compared to perturbative QCD calculations.

Contents

1 Introduction

Photoproduction of vector mesons (VMs) is usually thought of as a process where the photon fluctuates into a $q\bar{q}$ state, which then interacts with the proton and becomes a VM. If the spatial configuration of the $q\bar{q}$ state is large, its interaction with the proton is soft in nature and is usually described by Regge theory [1] together with the vector dominance model [2, 3]. This applies to exclusive photoproduction of the light VMs ρ, ω and ϕ (see Ivanov, Nikolaev and Savin [4] for a recent review). For heavy VMs, the $q\bar{q}$ pair is squeezed into a small configuration and perturbative QCD (pQCD) [5] can be applied. In exclusive photoproduction of J/ψ, $\gamma\,p \rightarrow J/\psi\,p$, the mass of the J/ψ provides a hard scale at the photon vertex and the small-size $q\bar{q}$ pair interacts through a two-gluon ladder with partons in the proton. If the four-momentum-transfer squared at the proton vertex is small, $|t| \lesssim 1\,\mathrm{GeV}^2$, and the proton stays intact, the cross section is predicted to fall exponentially with $|t|$.

When $|t|$ increases, $|t| > 1\,\text{GeV}^2$, the dominant process is that where the proton dissociates into a low-mass nucleon state Y,

$$\gamma\, p \rightarrow J/\psi\, Y. \tag{1.1}$$

At large $|t|$ values, the cross section is expected to have a power-law decrease with $|t|$ [6–9]. In addition, J/ψ photoproduction at large $|t|$ is a two-scale process in which the large mass of the heavy VM is the hard scale at the photon vertex and t is the hard scale at the proton vertex. At high photon-proton centre-of-mass energies, W, this process should be sensitive to BFKL [10–12] dynamics.

This paper contains results for the kinematic range $30 < W < 160\,\text{GeV}$ and $2 < |t| < 20\,\text{GeV}^2$, which is larger than for the previous ZEUS measurement [13]. The sample under study also represents more than a five-fold increase in integrated luminosity.

2 Experimental set-up

This analysis is based on data collected with the ZEUS detector at HERA in $1996-2000$. In those years HERA operated with an electron[1] beam energy of $27.5\,\text{GeV}$ and a proton beam energy, E_p, of $820\,\text{GeV}$ ($1996-1997$) and $920\,\text{GeV}$ ($1998-2000$). The data sample corresponds to an integrated luminosity of $112\,\text{pb}^{-1}$, $36\,\text{pb}^{-1}$ with $E_p = 820\,\text{GeV}$ and $76\,\text{pb}^{-1}$ with $E_p = 920\,\text{GeV}$.

A detailed description of the ZEUS detector can be found elsewhere [14]. A brief outline of the components that are most relevant for this analysis is given below.

Charged particles were tracked in the central tracking detector (CTD) [15–17], which operated in a magnetic field of $1.43\,\text{T}$ provided by a thin superconducting coil. The CTD consisted of 72 cylindrical drift chamber layers, organised in 9 superlayers covering the polar-angle[2] region $15° < \theta < 164°$. The transverse-momentum resolution for full-length tracks was $\sigma(p_T)/p_T = 0.0058 p_T \oplus 0.0065 \oplus 0.0014/p_T$, with p_T in GeV. The high-resolution uranium-scintillator calorimeter (CAL) [18–21] consisted of three parts: the forward (FCAL), the barrel (BCAL) and the rear (RCAL) calorimeters. Each part was subdivided transversely into towers and longitudinally into one electromagnetic section (EMC) and either one (in RCAL) or two (in BCAL and FCAL) hadronic sections (HAC). The smallest subdivision of the calorimeter is called a cell. The CAL energy resolutions, as measured under test-beam conditions, were $\sigma(E)/E = 0.18/\sqrt{E}$ for electrons and $\sigma(E)/E = 0.35/\sqrt{E}$ for hadrons, with E in GeV.

The muon system [22] consisted of tracking detectors (forward, barrel and rear muon chambers: FMUON, B/RMUON), which were placed inside and outside a magnetised iron yoke surrounding the CAL. The inner chambers, F/B/RMUI, covered the polar angles from $10°$ to $34°$, from $34°$ to $135°$ and from $135°$ to $171°$, respectively.

---

[1]Electrons and positrons are both referred to as electrons in this paper.

[2]The ZEUS coordinate system is a right-handed Cartesian system, with the Z axis pointing in the proton beam direction, referred to as the "forward direction", and the X axis pointing towards the centre of HERA. The coordinate origin is at the nominal interaction point.

The luminosity was determined from the rate of the bremsstrahlung process $ep \rightarrow e\gamma p$, where the photon was measured by a lead-scintillator calorimeter [23] located at $Z = -107\,\text{m}$.

3 Kinematics and reconstruction

The proton-dissociative J/ψ production process in ep interactions,

$$e(k)p(P) \rightarrow e(k')J/\psi(v)Y(P'),$$

is illustrated in figure 1. The signature of these events consists of two oppositely charged muons from the J/ψ decay and of the remnant of the dissociated proton. In the case of photoproduction, the beam electron is scattered at small angles and escapes undetected down the beampipe.

The variables k, k', P, P' and v are the four-momenta of the incident electron, scattered electron, incident proton, diffractive nucleonic system Y and J/ψ, respectively. The four-momentum of the exchanged photon is denoted by q. The kinematic variables are the following:

- $Q^2 = -q^2 = -(k - k')^2$, the negative squared four-momentum of the exchanged photon;

- $W^2 = (q + P)^2$, the squared centre-of-mass energy of the photon-proton system;

- $t = (P - P')^2 = (q - v)^2$, the squared four-momentum transfer at the proton vertex;

- $y = (P \cdot q)/(P \cdot k)$, the fraction of the electron energy transferred to the photon in the rest frame of the proton;

- $z = (P \cdot v)/(P \cdot q)$, the event inelasticity, i.e. the fraction of the virtual photon energy transferred to the J/ψ in the proton rest frame.

The dissociated proton either escapes undetected down the beampipe or deposits only a part of its energy in the CAL and hence the mass of the proton remnant, M_Y, cannot be measured precisely. However, M_Y is related to other kinematic variables through $M_Y^2 = W^2(1 - z) - |t|$.

The following angles are used to describe the decay of the J/ψ (see figure 2):

- Φ, the angle between the electron-scattering plane and the vector-meson plane, in the photon-proton centre-of-mass frame;

- θ_h and ϕ_h, the polar and azimuthal angles of the positively-charged decay particle in the helicity frame. Here, the helicity frame is the J/ψ rest frame and the quantisation axis is the meson direction in the photon-proton centre-of-mass system. The polar angle, θ_h, is defined as the angle between the direction of the positively charged decay particle and the quantisation axis. The azimuthal angle, ϕ_h, is the angle between the decay plane and the vector-meson production plane.

In this study, photoproduction is characterised by the non-observation of the scattered electron. Thus, Q^2 ranges from the kinematic minimum, $Q^2_{\min} = m_e^2 y^2/(1-y) \approx 10^{-7}\,\mathrm{GeV}^2$, where m_e is the electron mass, up to $Q^2_{\max} \approx 1\,\mathrm{GeV}^2$, the value at which the scattered electron becomes observable in the CAL. Since the mean Q^2 is small, $\langle Q^2 \rangle \approx 5 \cdot 10^{-5}\,\mathrm{GeV}^2$, it was neglected in the reconstruction of the other kinematic variables.

The variable t can be expressed as $t \approx -p_T^2$, where p_T is the transverse momentum of the produced vector meson in the laboratory frame. The variable W is calculated as $W^2 \approx 2E_p(E - p_Z)_{J/\psi}$, where E is the energy and p_Z is the longitudinal momentum of the vector meson. The quantities $(E - p_Z)_{J/\psi}$ and t were reconstructed using only the measured momenta of the VM muon decay particles.

The inelasticity z was computed from $z = (E - p_Z)_{J/\psi}/\sum(E - p_Z)$, where $\sum(E - p_Z) = (E - p_Z)_{J/\psi} + \sum(E - p_Z)_{\mathrm{had}}$ and $\sum(E - p_Z)_{\mathrm{had}}$ is reconstructed by summing over all the CAL energy deposits (larger than $300\,\mathrm{MeV}$) not associated with the J/ψ candidate.

4 Event selection

The events were selected online by the ZEUS three-level trigger system [14, 24]. The events were required to have at least one track in the CTD. At least one track had to point towards a CAL energy deposit compatible with a minimum ionising particle as well as a signal in the inner muon chambers.

The following was required offline:

- no scattered electron observed;

- two tracks with opposite charge pointing to a primary vertex with $|Z_{\mathrm{vertex}}| < 50\,\mathrm{cm}$;

- both tracks well reconstructed, i.e. traversing at least three superlayers in the CTD, including the innermost layer;

- each track associated with a distinct CAL energy deposit within a radius of $30\,\mathrm{cm}$;

- azimuthal angle between the two tracks associated with the two muon candidates less than $174°$ in order to reject cosmic-ray events;

- invariant mass of the two tracks, which were assigned a μ mass, in the range $2.6 < M_{\mu\mu} < 3.5\,\mathrm{GeV}$.

Events were required to be in a kinematic range where the properties of the final state particles were properly measured and the acceptance was well defined. This was satisfied for $2 < |t| < 20\,\mathrm{GeV}^2$ and $30 < W < 160\,\mathrm{GeV}$. The cut of $|t| > 2\,\mathrm{GeV}^2$ also significantly reduced the background from the exclusive process. A cut of $z > 0.95$ was applied to suppress non-diffractive background. This cut also restricted the invariant mass of the Y system to $M_Y < 30\,\mathrm{GeV}$.

The energy range $30 < W < 40\,\mathrm{GeV}$ was mainly populated by events triggered by the FMUON detector, while the range $40 < W < 160\,\mathrm{GeV}$ was dominated by B/RMUON-triggered events. The FMUON-triggered sample was limited to the data collected in $1996-1997$ and covered the $|t|$ region up to $10\,\mathrm{GeV}^2$.

After this selection procedure the number of observed di-muon events was 2817.

5 Theoretical predictions

The reaction $\gamma p \to J/\psi Y$ can be viewed as a three-step process. The photon fluctuates into a $q\bar{q}$ pair that scatters off a single parton in the proton by the exchange of a colour singlet. The scattered $q\bar{q}$ pair becomes a J/ψ and the struck parton and the proton remnant together fragment into the system Y. In lowest-order QCD the colour singlet exchanges a pair of gluons. In the leading logarithmic (LL) approximation, the process is described by the effective exchange of a gluon ladder.

As stated in the introduction, the process under study has two scales. At the photon vertex, where the photon fluctuates into a $q\bar{q}$ pair, the size is fixed and determined by the J/ψ mass. The second scale, $|t|$, controls the size of the system which emits the gluon ladder.

In the region where the scale $|t|$ is smaller than $M_{J/\psi}^2$ ($2 < |t| < 10\,\mathrm{GeV}^2$), the momenta on the gluon ladder are still expected to be ordered and thus a DGLAP [25–28] approach is appropriate. A calculation in this kinematic region has been carried out by Gotsman, Levin, Maor and Naftali (GLMN) [29], using their screening correction formalism and evolving the gluon in a LL DGLAP mechanism.

As $|t|$ increases, the BFKL mechanism is expected to dominate. The first LL BFKL calculations [6–8] were made using the Mueller-Tang (MT) approximation [30], which is only good for very large rapidity intervals. Enberg, Motyka and Poludniowski (EMP) [9] do not use the MT approximation and provide a complete analytical solution in LL for the case of heavy quarks (the case for any quark mass is discussed elsewhere [31, 32]). They use two different values of α_S as the pre-factor of the cross section and as the coupling relevant for the BFKL ladder. Enberg at al. [9] also present results of a non-leading (nonL) BFKL calculation.

In addition, a recent QCD calculation by Frankfurt, Strikman and Zhalov (FSZ) [33, 34] is motivated by the QCD factorisation theorem for large $|t|$ rapidity-gap processes and by the correspondence to exclusive J/ψ production at $|t| \sim 1\,\mathrm{GeV}^2$. In this QCD calculation in the triple-Pomeron limit, the W dependence of the cross section mainly depends on the gluon distribution of the proton.

In all models, a non-relativistic approximation of the J/ψ wave-function assuming equal sharing of longitudinal momenta between the quark and the anti-quark was used. The J/ψ retains the helicity of the photon which means that s-channel helicity is conserved (SCHC).

The DGLAP-motivated calculation predicts a mild W dependence of the cross section in the region of small $|t|$. In the region of larger $|t|$ the hard scale is chosen such that saturation is reached and thus the cross section is independent of W. The BFKL LL calculations predict a fast rise of the cross section with W which hardly depends on $|t|$. This is a unique feature of BFKL dynamics. The nonL BFKL model behaves in a similar way. In case of the FSZ parameterisation, the main energy dependence is provided by the behaviour of the gluon distribution.

All calculations predict an approximate power-law t-dependence of the cross section of the form $d\sigma/dt \sim |t|^{-n}$, where the value of n may depend on the $|t|$ range.

6 Monte Carlo and background evaluation

The acceptance and the effects of the detector response were determined using Monte Carlo (MC) events. All generated events were passed through the standard ZEUS detector simulation, based on GEANT 3.13 [35], the ZEUS trigger-simulation package and the same reconstruction and analysis programs as used for the data.

6.1 The process $ep \rightarrow e \, J/\psi \, Y$

The process $ep \rightarrow e \, J/\psi \, Y$ was modelled using the EPSOFT generator [36, 37]. The γp interactions were simulated assuming the exchange of a colourless object which couples to the whole proton, which subsequently fragments into a state Y. The particle multiplicities and the transverse momenta of the hadrons in the final state Y were simulated using parameterisations of pp data, while the longitudinal momenta were generated with a uniform rapidity distribution. The differential cross-section $d\sigma/dt$ was reweighted to obtain the shape observed in data. The assumption of s-channel helicity conservation was applied.

The differential cross section in M_Y^2 have the form $d\sigma/dM_Y^2 \propto (M_Y^2)^{-\beta(t,W)}$. The measured z distributions in $|t|$ and W bins were used to determine the $|t|$ and W dependence of the function $\beta(t,W)$. For each bin, a single value of the function β was extracted by using a χ^2 minimisation method. The results were parameterised in the form of $\beta(t,W) = (W/W_0)^{0.52\pm0.11} \exp((0.08 \pm 0.07) + (-0.14 \pm 0.03)|t|)$, with $W_0 = 95\,\mathrm{GeV}$. This parameterisation was used in all further studies.

6.2 Evaluation of background

The main sources of background were the non-resonant QED $\gamma\gamma$ processes, misidentified pion production and resonant background produced through the decay of the $\psi(2S)$ meson.

The non-resonant background due to the QED Bethe-Heitler di-muon production, $ep \rightarrow e\mu^+\mu^- Y$, was simulated using the GRAPE-DILEPTON 1.1 generator [38]. The background from $\gamma\gamma \rightarrow \mu^+\mu^-$ events was estimated in each bin by normalising to the luminosity of the data. The contribution of this background increased with $|t|$ from 6 to 10%.

The $\psi(2S)$ background was estimated using the DIPSI generator [39]. This background was dominated by the processes $\psi \rightarrow \pi^0\pi^0 J/\psi$ (BR=(16.84 $\pm$ 0.33)%) and $\psi \rightarrow \mu^+\mu^-$ (BR=(0.75 $\pm$ 0.08)%). It amounted to about 1% and 0.1%, respectively.

The background from exclusive J/ψ production was found [13] to be 5% for $2 < |t| < 3\,\mathrm{GeV}^2$. For $|t| > 3\,\mathrm{GeV}^2$, it was found to be consistent with zero. All background processes were subtracted bin-by-bin.

7 Systematic uncertainties

The systematic uncertainties were determined by varying the selection cuts and modifying the analysis procedure. Their effects on the integrated cross section are given in parentheses:

- the cut on Z vertex was changed by $\pm 10\,\mathrm{cm}$ ($+1.8\%$, -0.5%);

- the $\mu^+\mu^-$ mass window was changed to $2.8 - 3.4\,\mathrm{GeV}$ $(+0.2\%)$;

- instead of using the MC to subtract the background bin-by-bin, it was fitted with a polynomial function and statistically subtracted $(+1.5\%)$;

- the minimum energy of the CAL energy deposit included for the evaluation of the z variable was varied by $\pm100\,\mathrm{MeV}$ $(+0.3\%, -1.4\%)$;

- the strategy of matching energy deposits to the decay tracks was changed. Instead of matching every object within $30\,\mathrm{cm}$ from the track, only one island within this distance was matched to the track (-0.7%);

- the uncertainty of the muon acceptance, including the detector, the trigger and the reconstruction efficiency, was obtained from a study [40] based on an independent dimuon sample $(\pm6.3\%)$;

- the uncertainty on the acceptance due to modelling of the hadronic final state in the EPSOFT MC was estimated by varying the parameter β within its errors $(\pm2\%)$.

The overall systematic uncertainty was determined by adding all the individual uncertainties in quadrature. The uncertainty on the luminosity measurement, 2%, was not included.

8 Results

8.1 The J/ψ signal

The invariant-mass distribution of the $\mu^+\mu^-$ pairs is presented in figure 3. A clear peak at the J/ψ mass is observed with very little non-resonant background.

The distributions of the kinematic variables $|t|$, W, z, ϕ_h and $\cos\theta_h$ are shown in figure 4. The MC distributions of the J/ψ events are shown as well as the QED background. The overall agreement between data and MC is good.

8.2 Determination of photon-proton cross-section

The ep cross section was determined by subtracting the background from the data, correcting for the acceptance, using the branching ratio for the muon channel decay $(5.88\pm0.10\%)$ and using the measured luminosity.

Photon-proton cross sections were extracted from the ep cross sections by using photon flux factors. The flux factors [41] generated at the leptonic vertex relate the ep and the γp cross sections by

$$\frac{d^2\sigma^{ep\to eJ/\psi Y}}{dydQ^2} = \Gamma_T(y, Q^2)\sigma^{\gamma p}(y),$$

where Γ_T is the effective photon flux. The cross sections for different beam energies were averaged using the corresponding luminosities.

8.3 |t| dependence

Differential γp cross section $d\sigma/dt$ for proton-dissociative J/ψ photoproduction was measured in the kinematic region $30 < W < 160\,\text{GeV}$, $2 < |t| < 20\,\text{GeV}^2$ and $z > 0.95$.

The differential cross section as a function of $|t|$ is shown in figure 5 and listed in table 1. The cross section falls steeply with $|t|$. The data cannot be described in the whole $|t|$ region by one exponential function of the form $\sim e^{-b|t|}$, where b is a constant. Neither does a single power-law dependence of the form $|t|^{-n}$, where n is a constant, fit the data. A good fit can, however, be obtained by fitting two $|t|$ ranges separately, giving $n = 1.9 \pm 0.1$ for $2 < |t| < 5\,\text{GeV}^2$ and $n = 3.0 \pm 0.1$ for $5 < |t| < 20\,\text{GeV}^2$. Note that a good fit can also be obtained to a quadratic exponential function $e^{-b|t|+c|t|^2}$.

The differential cross-section $d\sigma/dt$ as a function of $|t|$ is shown again in figure 6, together with the H1 data [43], and compared with different theoretical models. The GLMN LL model gives a good description of the data up to about $|t| = 5\,\text{GeV}^2$, but falls off slower than the data up to the region where the calculation is valid ($|t| < 10\,\text{GeV}^2$). The EMP LL prediction, using $\alpha_S = 0.205$ in the pre-factor and $\alpha_S = 0.16$ in the BFKL evolution, lies below the data in the whole range of $|t|$. The FSZ results are shown for a calculation using a Pomeron trajectory with intercept of 1.1 and a slope of $0.005\,\text{GeV}^{-2}$. Similar results are obtained with a Pomeron intercept of 1.0. The CTEQ6M parameterisation [42] of the parton density functions is used. The FSZ calculation describes the data well up to $|t|$ of about $12\,\text{GeV}^2$ but falls-off too steeply at larger $|t|$ values.

8.4 W dependence

In the Regge formalism, the differential cross section can be expressed as

$$d\sigma/dt = F(t)W^{4(\alpha_{I\!P}(t)-1)}, \tag{8.1}$$

where $F(t)$ is a function of t and $\alpha_{I\!P}(t)$ is the effective Pomeron trajectory. This expression is usually used for exclusive reactions, but has been used also for the case where M_Y is integrated over [13, 43]. By studying the W dependence of $d\sigma/dt$ at fixed t, the Pomeron trajectory can be determined.

The W dependence of the differential cross section $d\sigma/dt$ for eight fixed t values is shown in figure 7 and listed in table 2. At each t value the cross section is parameterised as $\sigma \sim W^\delta$ and the lines in the figure are the result of these fits. The values of $\alpha_{I\!P}$ can be obtained at each t value through

$$\alpha_{I\!P} = (\delta + 4)/4 \tag{8.2}$$

and are shown in figure 8. The values of δ and of $\alpha_{I\!P}$ are listed in table 3. A linear fit of the form

$$\alpha_{I\!P}(t) = \alpha_{I\!P}(0) + \alpha'_{I\!P} \cdot t \tag{8.3}$$

yields an intercept

$$\alpha_{I\!P}(0) = 1.084 \pm 0.031(\text{stat.})^{+0.025}_{-0.018}(\text{syst.}), \tag{8.4}$$

and a slope

$$\alpha'_{I\!P} = -0.014 \pm 0.007(\text{stat.})^{+0.004}_{-0.005}(\text{syst.}). \tag{8.5}$$

The value of the intercept is consistent with that of the so-called "soft" Pomeron [44] (1.0808). The slope is different from that of the "soft" Pomeron [45] ($0.25 \, \text{GeV}^{-2}$), but is consistent with the predictions of the BFKL Pomeron [46, 47].

The γp cross section as a function of W was measured in four bins of $|t|$: $2 < |t| < 3 \, \text{GeV}^2$; $3 < |t| < 5 \, \text{GeV}^2$; $5 < |t| < 10 \, \text{GeV}^2$ and $10 < |t| < 20 \, \text{GeV}^2$ for $30 < W < 160 \, \text{GeV}$. The cross-section values are shown in figure 9 and summarised in table 4. The H1 data [43] for the $|t|$ bin of 5 to $10 \, \text{GeV}^2$ are also shown. A clear rise with W is seen in all the four $|t|$ regions. Also shown in the figure are the predictions of the models used in the comparison with $d\sigma/dt$. The DGLAP-based GLMN LL calculation agrees well with the data in the first two $|t|$ bins, but fails to describe the rise with W for $|t| > 5 \, \text{GeV}^2$. The other two calculations, EMP LL and FSZ, predict a W dependence which is too steep in all the $|t|$ ranges presented in the analysis.

The measurements of the present analysis, both the differential cross section as a function of $|t|$ and the W dependence of the cross section, are in good agreement with those of the H1 collaboration [43] in the common kinematic region.

8.5 Decay angular distributions

The angular distributions of the J/ψ decay provide information about the photon and J/ψ polarisation states. The normalised two-dimensional angular distributions can be written in terms of spin density matrix elements, r, as:

$$\frac{1}{\sigma} \frac{d^2\sigma}{d\cos\theta_h d\phi_h} = \frac{3}{4\pi} \left(\frac{1}{2}(1 + r_{00}^{04}) - \frac{1}{2}(3r_{00}^{04} - 1)\cos^2\theta_h + \right.$$
$$\left. + \sqrt{2}\text{Re}\{r_{10}^{04}\}\sin 2\theta_h \cos\phi_h + r_{1-1}^{04}\sin^2\theta_h \cos 2\phi_h \right). \tag{8.6}$$

The one-dimensional distributions result from the integration over θ_h or ϕ_h and are expressed as:

$$\frac{d\sigma}{d\cos\theta_h} \propto 1 + r_{00}^{04} + (1 - 3r_{00}^{04})\cos^2\theta_h \tag{8.7}$$

and

$$\frac{d\sigma}{d\phi} \propto 1 + r_{1-1}^{04}\cos 2\phi_h. \tag{8.8}$$

The spin density matrix element r_{00}^{04} represents the probability that the produced J/ψ has helicity zero, $\text{Re}\{r_{10}^{04}\}$ is proportional to the single-flip amplitude and r_{1-1}^{04} is related to the interference between non-flip and double-flip amplitudes. If SCHC holds, the J/ψ retains the helicity of the almost real photon and all the three matrix elements are expected to be zero.

The distributions of $\cos\theta_h$ and ϕ_h after background subtraction and acceptance corrections in four $|t|$ bins and for $30 < W < 160 \, \text{GeV}$ are shown in figure 10. They were fitted using formulae (8.7) and (8.8). The r_{00}^{04}, $\text{Re}\{r_{10}^{04}\}$ and r_{1-1}^{04} spin density matrix elements were extracted from a two-dimensional χ^2 minimisation fit using eq. (8.6) and are summarised in table 5 and shown in figure 11. The results for r_{00}^{04} and r_{1-1}^{04} are compatible

with zero. The values obtained for $\mathrm{Re}\{r^{04}_{10}\}$ are not compatible with zero for $|t| < 10\,\mathrm{GeV}^2$, contrary to the expectation from SCHC.

The measurements of the present analysis, the differential cross section as a function of $|t|$, the W dependence of the cross section and the density matrix elements, are in good agreement with those of the H1 collaboration [43] within the common kinematic region.

9 Summary

Proton-dissociative J/ψ production was measured at HERA in the photoproduction regime in the kinematic region $30 < W < 160\,\mathrm{GeV}$, $z > 0.95$ and $2 < |t| < 20\,\mathrm{GeV}^2$.

The $|t|$ dependence of the differential cross section, $d\sigma/d|t|$, is found to be approximately power-like, $\sim |t|^{-n}$, with the power n increasing with $|t|$.

The effective Pomeron trajectory was derived from a measurement of the W dependence of the cross section at fixed t values. The value of the slope of the trajectory is compatible with zero. It is consistent with the predictions of the BFKL Pomeron but different from the slope of the "soft" Pomeron.

The cross-section $\sigma(\gamma p \rightarrow J/\psi\ Y)$ rises significantly with W in each $|t|$ bin. The t and W dependence of the cross section were compared to several theoretical calculations. The DGLAP-motivated GLMN LL [29] calculation can describe the behaviour of the data, both in t and in W, up to $|t| = 5\,\mathrm{GeV}^2$. The BFKL-motivated EMP LL [9] calculation fails to describe the data in the kinematic region of the present measurement. The FSZ [33, 34] calculation describes the t dependence of the cross section only up to $|t| = 12\,\mathrm{GeV}^2$ and fails to reproduce the W dependence.

The spin density matrix elements of the J/ψ, r^{04}_{00} and r^{04}_{1-1} are consistent with zero, as expected from s-channel helicity conservation. The values obtained for $\mathrm{Re}\{r^{04}_{10}\}$ are not compatible with zero for $|t| < 10\,\mathrm{GeV}^2$, contrary to the expectation from SCHC.

Acknowledgments

| $\lvert t \rvert$ bin | | | $\langle \lvert t \rvert \rangle$ | $d\sigma/d\lvert t \rvert$ |
$(\,\mathrm{GeV}^2)$			$(\,\mathrm{GeV}^2)$	$(\,\mathrm{nb}/\,\mathrm{GeV}^2)$
2.0	−	3.0	2.5	$6.05 \pm 0.23\ ^{+0.60}_{-0.43}$
3.0	−	4.0	3.5	$3.14 \pm 0.18\ ^{+0.29}_{-0.23}$
4.0	−	5.0	4.4	$1.91 \pm 0.13\ ^{+0.17}_{-0.18}$
5.0	−	6.5	5.6	$0.97 \pm 0.08\ ^{+0.11}_{-0.10}$
6.5	−	8.0	7.2	$0.41 \pm 0.05\ ^{+0.06}_{-0.03}$
8.0	−	11.0	9.3	$0.21 \pm 0.02\ ^{+0.04}_{-0.02}$
11.0	−	14.0	12.4	$0.07 \pm 0.01\ ^{+0.02}_{-0.01}$
14.0	−	20.0	16.5	$0.05 \pm 0.01\ ^{+0.01}_{-0.01}$

Table 1. Differential cross-section $d\sigma/d\lvert t \rvert$ as a function of $\lvert t \rvert$ for $30 < W < 160\,\mathrm{GeV}$ and $z > 0.95$. The first uncertainty is statistical and the second is systematic.

$\lvert t\rvert$ bin (GeV^2)	$-t$ (GeV^2)	W bin (GeV)		$\langle W\rangle$ (GeV)	$d\sigma/dt$ (nb/ GeV^2)
		30 − 50		39.5	$3.82 \pm 0.59\ ^{+0.68}_{-0.51}$
		50 − 70		59.5	$6.65 \pm 0.61\ ^{+0.58}_{-0.65}$
		70 − 80		75.0	$8.52 \pm 1.10\ ^{+0.90}_{-0.98}$
		80 − 90		84.8	$5.95 \pm 0.91\ ^{+0.65}_{-0.51}$
2.0−2.5	2.2	90 − 100		95.0	$7.10 \pm 1.08\ ^{+0.57}_{-1.18}$
		100 − 110		105.1	$7.51 \pm 1.13\ ^{+0.89}_{-0.70}$
		110 − 120		114.9	$6.83 \pm 1.20\ ^{+0.99}_{-0.58}$
		120 − 130		125.1	$8.79 \pm 1.52\ ^{+0.98}_{-0.78}$
		130 − 160		144.0	$6.74 \pm 0.93\ ^{+1.25}_{-0.63}$
		30 − 50		39.6	$2.47 \pm 0.52\ ^{+0.60}_{-0.31}$
		50 − 70		59.3	$3.93 \pm 0.50\ ^{+0.37}_{-0.53}$
		70 − 80		74.8	$5.43 \pm 0.91\ ^{+0.74}_{-0.91}$
		80 − 90		85.0	$4.52 \pm 0.84\ ^{+0.67}_{-0.73}$
2.5−3.0	2.7	90 − 100		95.0	$4.89 \pm 0.93\ ^{+0.56}_{-0.32}$
		100 − 110		104.8	$4.81 \pm 0.95\ ^{+0.51}_{-0.53}$
		110 − 120		114.7	$6.02 \pm 1.26\ ^{+0.71}_{-0.64}$
		120 − 130		124.9	$6.34 \pm 1.33\ ^{+1.08}_{-0.65}$
		130 − 160		144.5	$7.00 \pm 1.17\ ^{+0.92}_{-0.68}$
		30 − 50		39.7	$2.06 \pm 0.34\ ^{+0.29}_{-0.30}$
		50 − 70		59.5	$2.65 \pm 0.30\ ^{+0.23}_{-0.13}$
		70 − 80		74.8	$3.33 \pm 0.53\ ^{+0.30}_{-0.33}$
3.0−4.0	3.4	80 − 90		84.8	$3.17 \pm 0.53\ ^{+0.34}_{-0.45}$
		90 − 110		99.8	$3.38 \pm 0.45\ ^{+0.36}_{-0.21}$
		110 − 130		119.6	$3.72 \pm 0.54\ ^{+0.32}_{-0.30}$
		130 − 160		143.5	$3.26 \pm 0.52\ ^{+0.49}_{-0.38}$

Table 2. Differential cross section as a function of W in eight t bins and for $z > 0.95$. The first uncertainty is statistical and the second is systematic.

$\lvert t \rvert$ bin (GeV^2)	$-t$ (GeV^2)	W bin (GeV)			$\langle W \rangle$ (GeV)	$d\sigma/dt$ (nb/GeV^2)
4.0−5.0	4.5	30	−	50	39.5	$0.95 \pm 0.23\,^{+0.08}_{-0.18}$
		50	−	70	59.8	$1.51 \pm 0.22\,^{+0.10}_{-0.17}$
		70	−	80	74.8	$1.97 \pm 0.38\,^{+0.15}_{-0.22}$
		80	−	90	85.1	$1.98 \pm 0.39\,^{+0.23}_{-0.34}$
		90	−	110	99.6	$1.71 \pm 0.29\,^{+0.24}_{-0.30}$
		110	−	130	119.7	$2.44 \pm 0.44\,^{+0.44}_{-0.29}$
		130	−	160	144.5	$2.82 \pm 0.51\,^{+0.37}_{-0.52}$
5.0−6.5	5.7	30	−	70	48.1	$0.45 \pm 0.15\,^{+0.08}_{-0.07}$
		50	−	70	59.6	$0.79 \pm 0.14\,^{+0.11}_{-0.07}$
		70	−	90	79.9	$1.00 \pm 0.15\,^{+0.12}_{-0.16}$
		90	−	110	100.0	$1.07 \pm 0.19\,^{+0.12}_{-0.15}$
		110	−	160	134.1	$1.20 \pm 0.17\,^{+0.17}_{-0.13}$
6.5−8.0	7.2	30	−	70	47.7	$0.17 \pm 0.11\,^{+0.02}_{-0.02}$
		50	−	70	60.0	$0.28 \pm 0.08\,^{+0.05}_{-0.08}$
		70	−	90	79.4	$0.22 \pm 0.07\,^{+0.07}_{-0.01}$
		90	−	110	99.8	$0.43 \pm 0.11\,^{+0.08}_{-0.06}$
		110	−	160	133.6	$0.64 \pm 0.13\,^{+0.12}_{-0.06}$
8.0−11.0	9.2	50	−	70	59.5	$0.12 \pm 0.04\,^{+0.03}_{-0.01}$
		70	−	90	80.4	$0.24 \pm 0.05\,^{+0.05}_{-0.03}$
		90	−	110	99.6	$0.21 \pm 0.06\,^{+0.05}_{-0.04}$
		110	−	160	133.4	$0.26 \pm 0.05\,^{+0.04}_{-0.03}$
11.0−20.0	14.2	50	−	70	59.8	$0.04 \pm 0.01\,^{+0.01}_{-0.01}$
		70	−	90	79.3	$0.05 \pm 0.01\,^{+0.01}_{-0.01}$
		90	−	110	100.0	$0.07 \pm 0.02\,^{+0.02}_{-0.02}$
		110	−	160	133.9	$0.07 \pm 0.02\,^{+0.02}_{-0.01}$

Table 2 (continuation): Differential cross section as a function of W in eight t bins and for $z > 0.95$. The first uncertainty is statistical and the second is systematic.

$|t|$ bin (GeV^2)		$-t$ (GeV^2)	δ	$\alpha_{I\!P}$
2.0	–	2.5	2.2	$0.38 \pm 0.10 \ ^{+0.11}_{-0.06}$	$1.10 \pm 0.03 \ ^{+0.03}_{-0.02}$
2.5	–	3.0	2.7	$0.70 \pm 0.15 \ ^{+0.10}_{-0.10}$	$1.18 \pm 0.04 \ ^{+0.02}_{-0.02}$
3.0	–	4.0	3.4	$0.39 \pm 0.13 \ ^{+0.08}_{-0.07}$	$1.10 \pm 0.03 \ ^{+0.02}_{-0.02}$
4.0	–	5.0	4.5	$0.72 \pm 0.18 \ ^{+0.08}_{-0.07}$	$1.18 \pm 0.05 \ ^{+0.02}_{-0.02}$
5.0	–	6.5	5.7	$0.70 \pm 0.21 \ ^{+0.12}_{-0.12}$	$1.18 \pm 0.05 \ ^{+0.03}_{-0.03}$
6.5	–	8.0	7.2	$1.38 \pm 0.46 \ ^{+0.37}_{-0.24}$	$1.35 \pm 0.12 \ ^{+0.09}_{-0.06}$
8.0	–	11.0	9.2	$0.78 \pm 0.38 \ ^{+0.06}_{-0.12}$	$1.20 \pm 0.09 \ ^{+0.02}_{-0.03}$
11.0	–	20.0	14.2	$0.82 \pm 0.44 \ ^{+0.34}_{-0.08}$	$1.21 \pm 0.11 \ ^{+0.09}_{-0.02}$

Table 3. The values of the parameters δ and the effective Pomeron trajectory $\alpha_{I\!P}$ for eight fixed t values. The first uncertainty is statistical and the second is systematic.

$\|t\|$ bin (GeV^2)	$-t$ (GeV^2)	W bin (GeV)		$\langle W \rangle$ (GeV)	$d\sigma/dt$ ($\mathrm{nb}/\mathrm{GeV}^2$)
$2-3$	2.5	30	50	39.5	$3.23 \pm 0.40\ ^{+0.43}_{-0.33}$
		50	70	59.4	$5.35 \pm 0.40\ ^{+0.31}_{-0.34}$
		70	80	74.9	$7.13 \pm 0.72\ ^{+0.74}_{-0.49}$
		80	90	84.9	$5.30 \pm 0.62\ ^{+0.47}_{-0.50}$
		90	100	95.0	$6.04 \pm 0.71\ ^{+0.37}_{-0.45}$
		100	110	105.0	$6.28 \pm 0.75\ ^{+0.57}_{-0.37}$
		110	120	114.8	$6.42 \pm 0.86\ ^{+0.57}_{-0.41}$
		120	130	125.1	$7.52 \pm 1.00\ ^{+0.77}_{-0.60}$
		130	160	144.3	$6.80 \pm 0.72\ ^{+0.71}_{-0.57}$
$3-5$	3.8	30	50	39.7	$3.10 \pm 0.42\ ^{+0.21}_{-0.20}$
		50	70	59.6	$4.23 \pm 0.37\ ^{+0.22}_{-0.23}$
		70	80	74.9	$5.28 \pm 0.65\ ^{+0.31}_{-0.36}$
		80	90	84.9	$5.22 \pm 0.67\ ^{+0.48}_{-0.45}$
		90	100	94.9	$4.29 \pm 0.63\ ^{+0.41}_{-0.26}$
		100	110	105.0	$6.42 \pm 0.93\ ^{+0.68}_{-0.42}$
		110	120	115.0	$5.79 \pm 0.92\ ^{+0.39}_{-0.32}$
		120	130	125.0	$6.55 \pm 1.07\ ^{+0.54}_{-0.53}$
		130	160	143.9	$6.40 \pm 0.75\ ^{+0.77}_{-0.63}$
$5-10$	6.7	30	70	53.9	$1.69 \pm 0.20\ ^{+0.14}_{-0.14}$
		70	90	79.9	$2.36 \pm 0.28\ ^{+0.20}_{-0.25}$
		90	110	99.9	$2.69 \pm 0.35\ ^{+0.18}_{-0.23}$
		110	160	133.8	$3.61 \pm 0.36\ ^{+0.34}_{-0.28}$
$10-20$	13.3	50	80	63.9	$0.50 \pm 0.108\ ^{+0.05}_{-0.07}$
		80	120	98.8	$0.72 \pm 0.132\ ^{+0.07}_{-0.12}$
		120	160	139.8	$0.84 \pm 0.188\ ^{+0.14}_{-0.10}$

Table 4. The cross-section $\sigma(\gamma p \to J/\psi\, Y)$ as a function of W in four $|t|$ bins and for $z > 0.95$. The first uncertainty is statistical and the second is systematic.

$\|t\|$ bin (GeV^2)	$\langle \|t\| \rangle$ (GeV^2)	r^{04}_{1-1}	r^{04}_{00}	$Re\{r^{04}_{10}\}$
$2 - 3$	2.5	$0.005 \pm 0.064\ ^{+0.019}_{-0.024}$	$0.090 \pm 0.088\ ^{+0.009}_{-0.017}$	$0.117 \pm 0.061\ ^{+0.025}_{-0.019}$
$3 - 5$	3.8	$-0.206 \pm 0.072\ ^{+0.021}_{-0.037}$	$-0.030 \pm 0.100\ ^{+0.041}_{-0.083}$	$0.197 \pm 0.068\ ^{+0.046}_{-0.055}$
$5 - 10$	6.7	$0.003 \pm 0.106\ ^{+0.036}_{-0.016}$	$-0.033 \pm 0.147\ ^{+0.020}_{-0.042}$	$0.154 \pm 0.088\ ^{+0.016}_{-0.025}$
$10 - 20$	13.3	$-0.164 \pm 0.240\ ^{+0.108}_{-0.115}$	$-0.259 \pm 0.328\ ^{+0.081}_{-0.062}$	$-0.153 \pm 0.172\ ^{+0.062}_{-0.047}$

Table 5. The spin density matrix elements for $30 < W < 160\,\mathrm{GeV}$ and $z > 0.95$. The first uncertainty is statistical and the second is systematic.
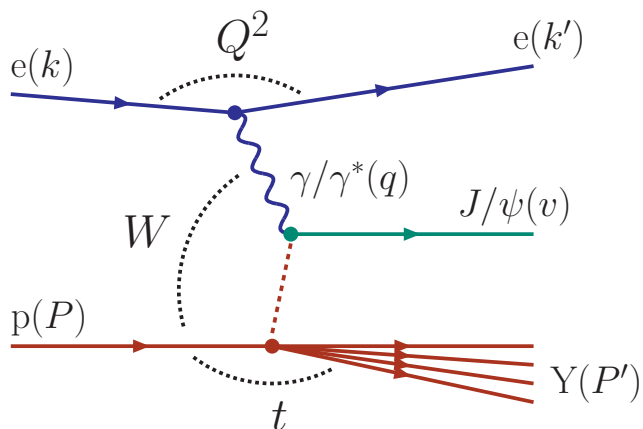
Figure 1. Schematic diagram of proton-dissociative J/ψ production in ep interactions, $ep \to eJ/\psi\, Y$.
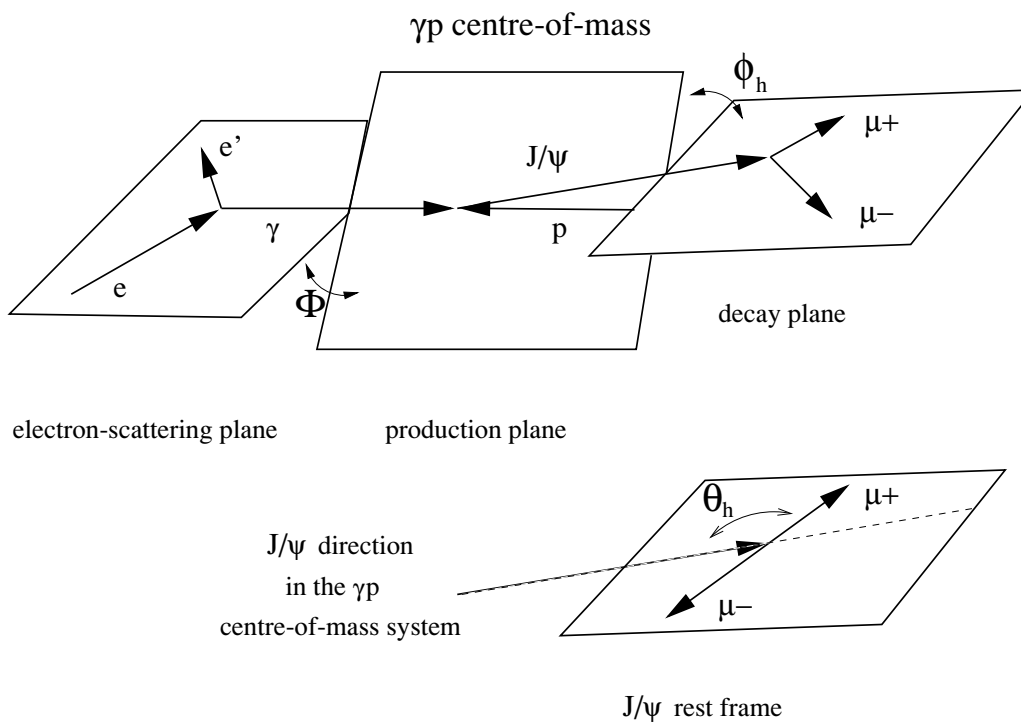
Figure 2. Angles used to analyse the helicity states of the J/ψ, see text.
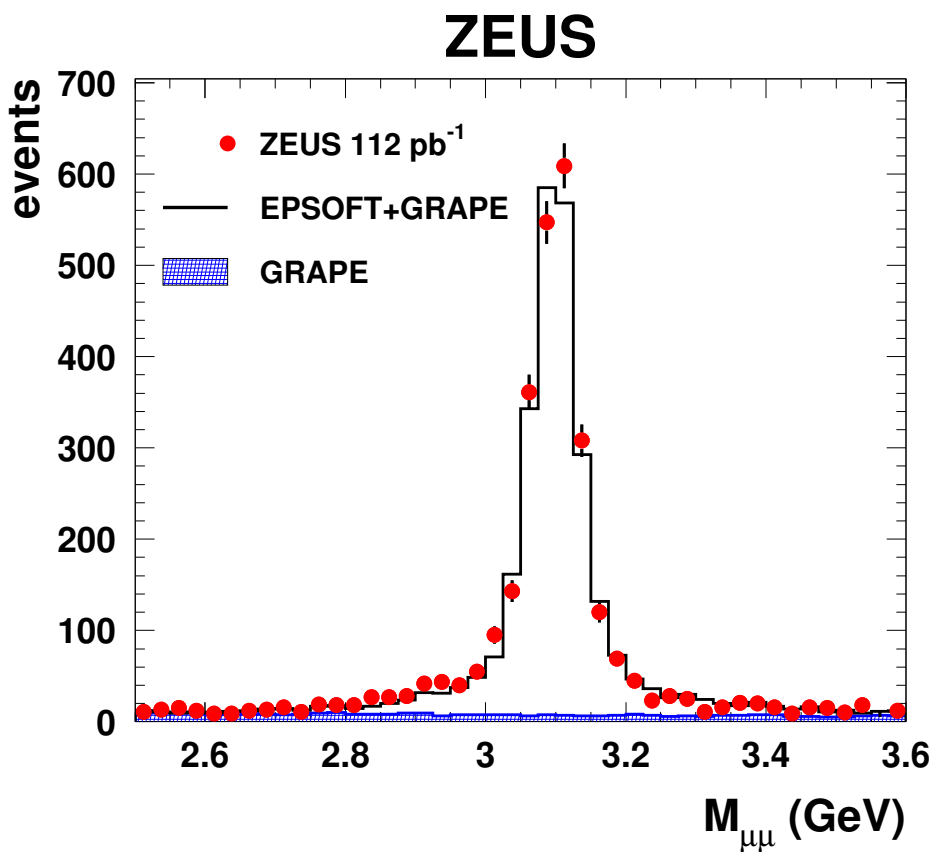
Figure 3. The invariant-mass spectrum for $\mu^+\mu^-$ pairs in the range $30 < W < 160\,\text{GeV}$, $2 < |t| < 20\,\text{GeV}^2$ and $z > 0.95$. Error bars represent only statistical uncertainties. The data are compared to the MC distributions. The hatched histogram represents the $ep \to e\mu^+\mu^-Y$ background as simulated by the GRAPE MC. The solid-line histogram represents the sum of J/ψ and background MC events.
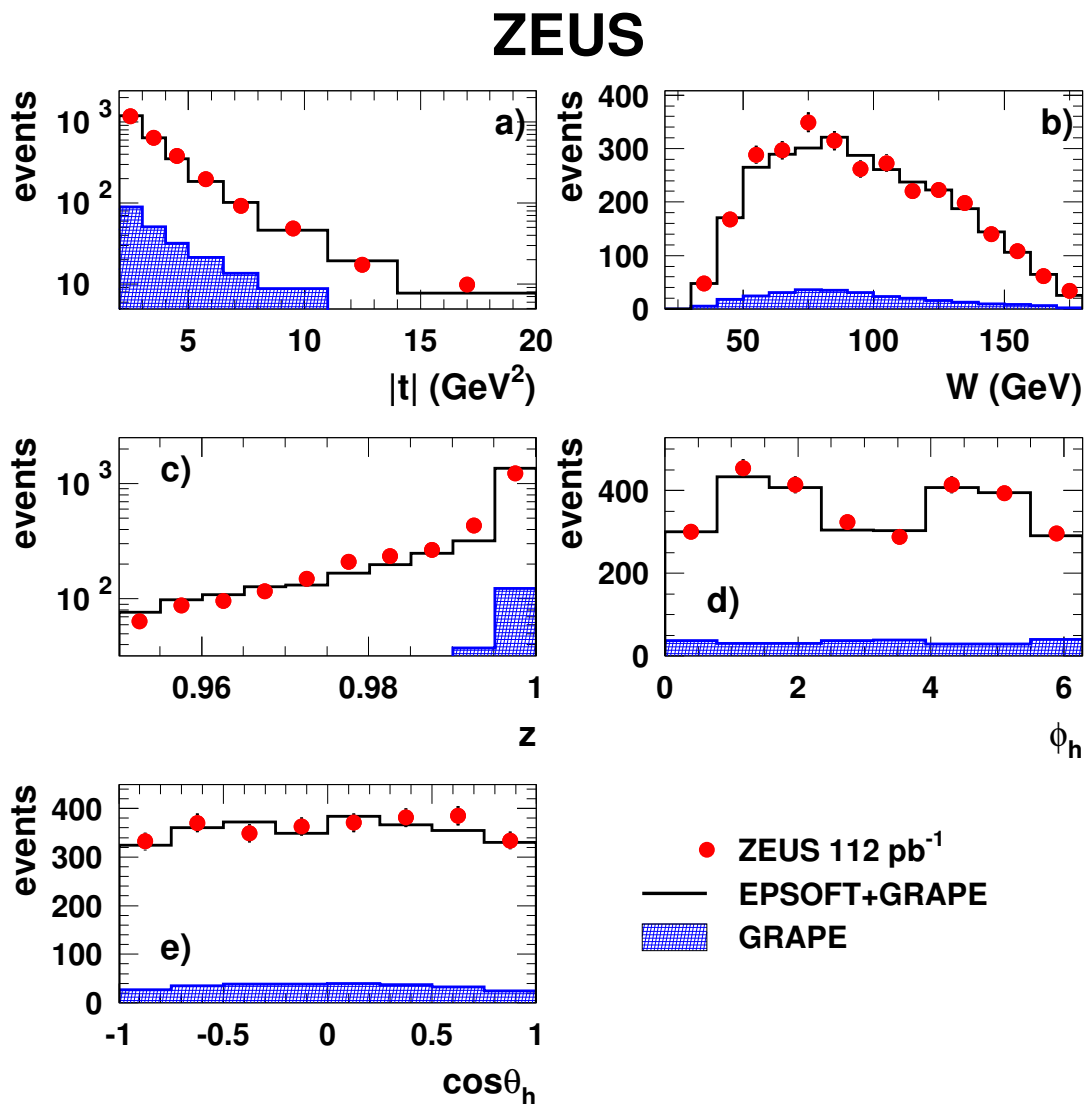
Figure 4. Comparison between the data and MC distributions in the range $30 < W < 160$ GeV, $2 < |t| < 20$ GeV^2 and $z > 0.95$ for a) $|t|$, b) W, c) z, d) ϕ_h, e) $\cos\theta_h$. Error bars represent only statistical uncertainties. The hatched histograms represent the $ep \rightarrow e\mu^+\mu^-Y$ background as simulated by the GRAPE MC. The solid-line histogram represents the sum of J/ψ and background MC events.
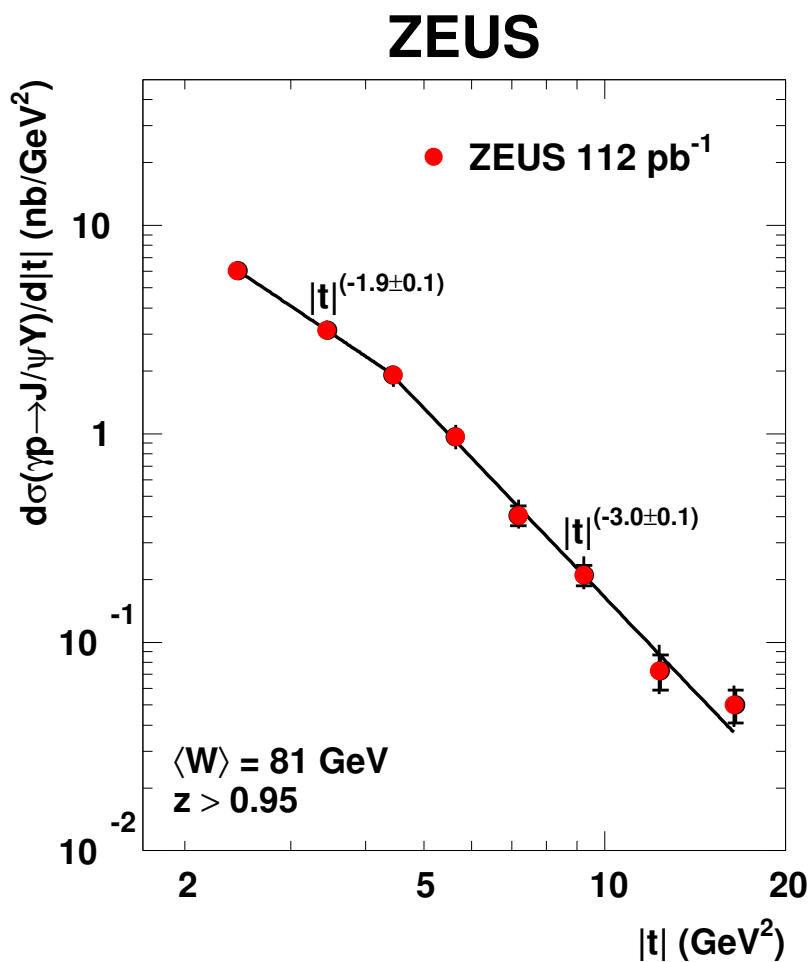
Figure 5. The $|t|$ dependence of the differential cross-section $d\sigma/d|t|$ for the process $\gamma p \to J/\psi\, Y$ at $\langle W \rangle = 81\,\text{GeV}$ and $z > 0.95$. The inner bars correspond to the statistical uncertainties and the outer to the statistical and systematic uncertainties added in quadrature. The solid lines are the results of power fits to the form $d\sigma/dt \sim |t|^n$.
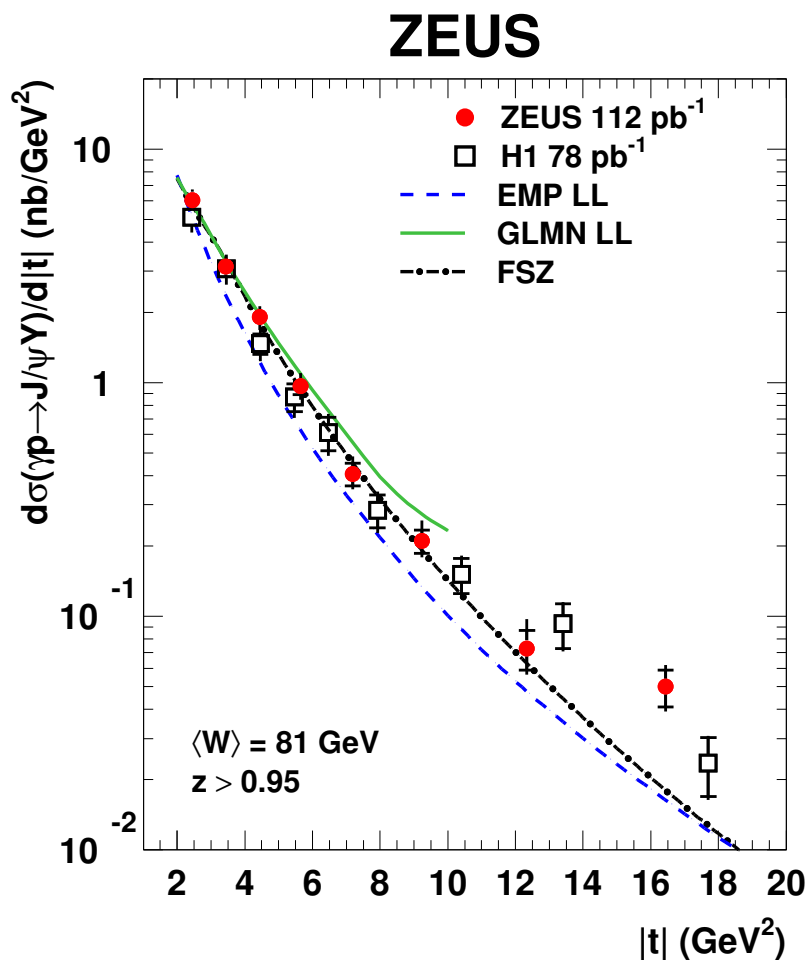
Figure 6. The $|t|$ dependence of the differential cross-section $d\sigma/d|t|$ for the process $\gamma p \to J/\psi\, Y$ at $\langle W \rangle = 81\,\text{GeV}$ and $z > 0.95$. The H1 data, $50 < W < 150\,\text{GeV}$, [43] are also shown. The inner bars correspond to the statistical uncertainties and the outer to the statistical and systematic uncertainties added in quadrature. The lines show the predictions of several calculations, referred to in the text.
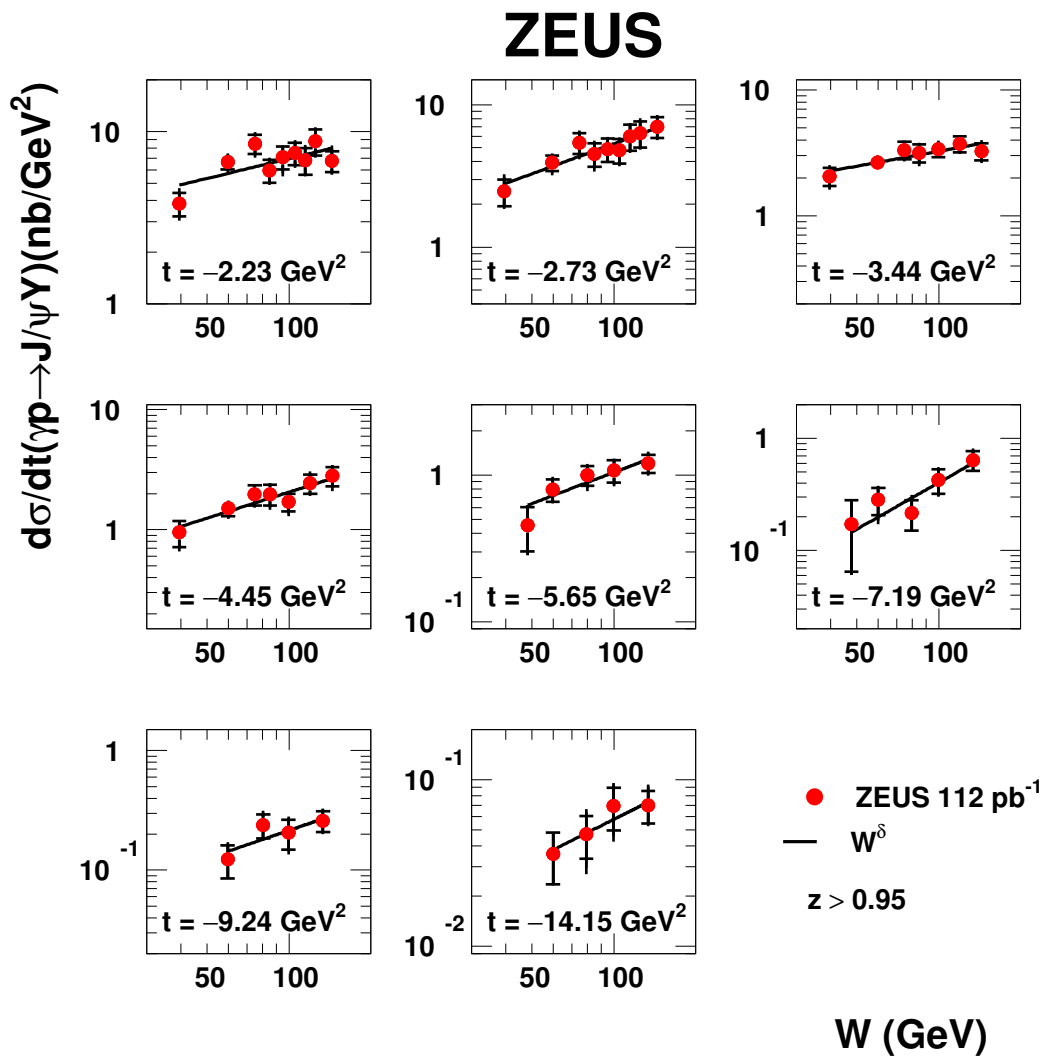
Figure 7. The W dependence of the differential cross-section $d\sigma/dt$ for the process $\gamma p \to J/\psi\ Y$ ($z > 0.95$) at fixed $|t|$ values, as indicated in the figure. The inner bars correspond to the statistical uncertainties and the outer to the statistical and systematic uncertainties added in quadrature. The solid lines are the results of fits to the form $d\sigma/dt \sim W^\delta$.
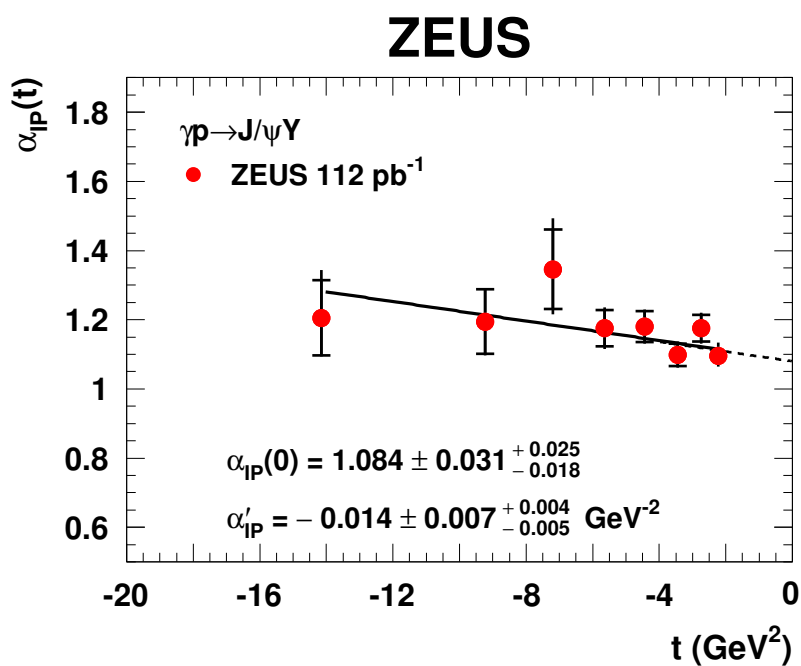
Figure 8. The effective Pomeron trajectory as a function of t. The inner bars correspond to the statistical uncertainties and the outer to the statistical and systematic uncertainties added in quadrature. The solid line is a fit of the form $\alpha_{I\!P}(t) = \alpha_{I\!P}(0) + \alpha'_{I\!P} \cdot t$. The dashed line is an extrapolation to $\alpha_{I\!P}(0)$.
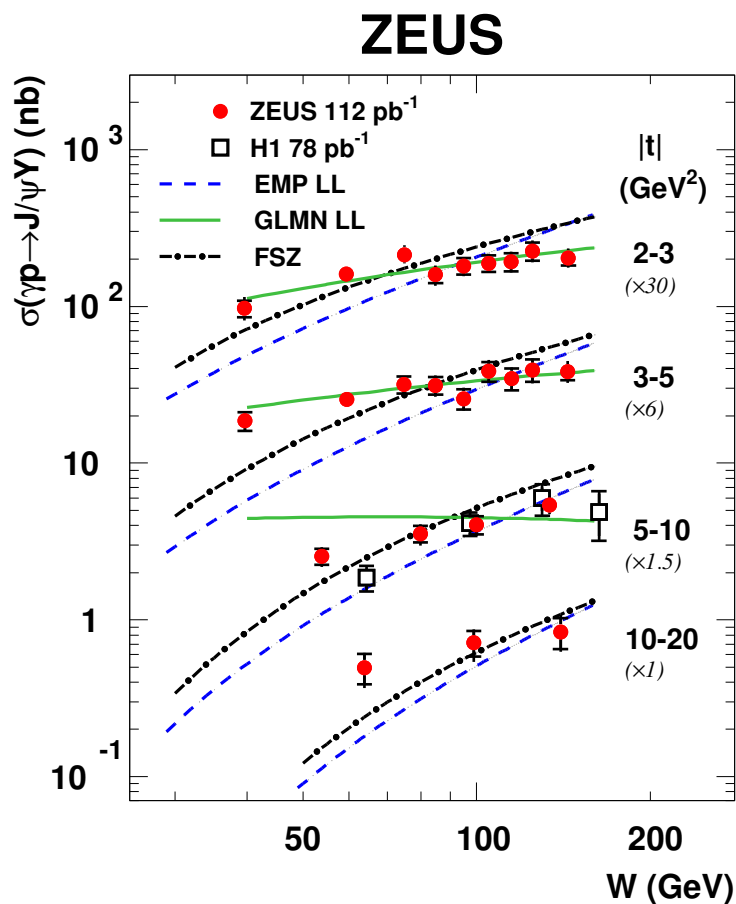
Figure 9. The W dependence for the process $\gamma p \to J/\psi\, Y$ ($z > 0.95$) in four different $|t|$ bins. The H1 data [43] for the $|t|$ bin of 5 to $10\,\text{GeV}^2$ are also shown. The inner bars correspond to the statistical uncertainties and the outer to the statistical and systematic uncertainties added in quadrature. The lines show the predictions of several calculations referred to in the text.

ZEUS
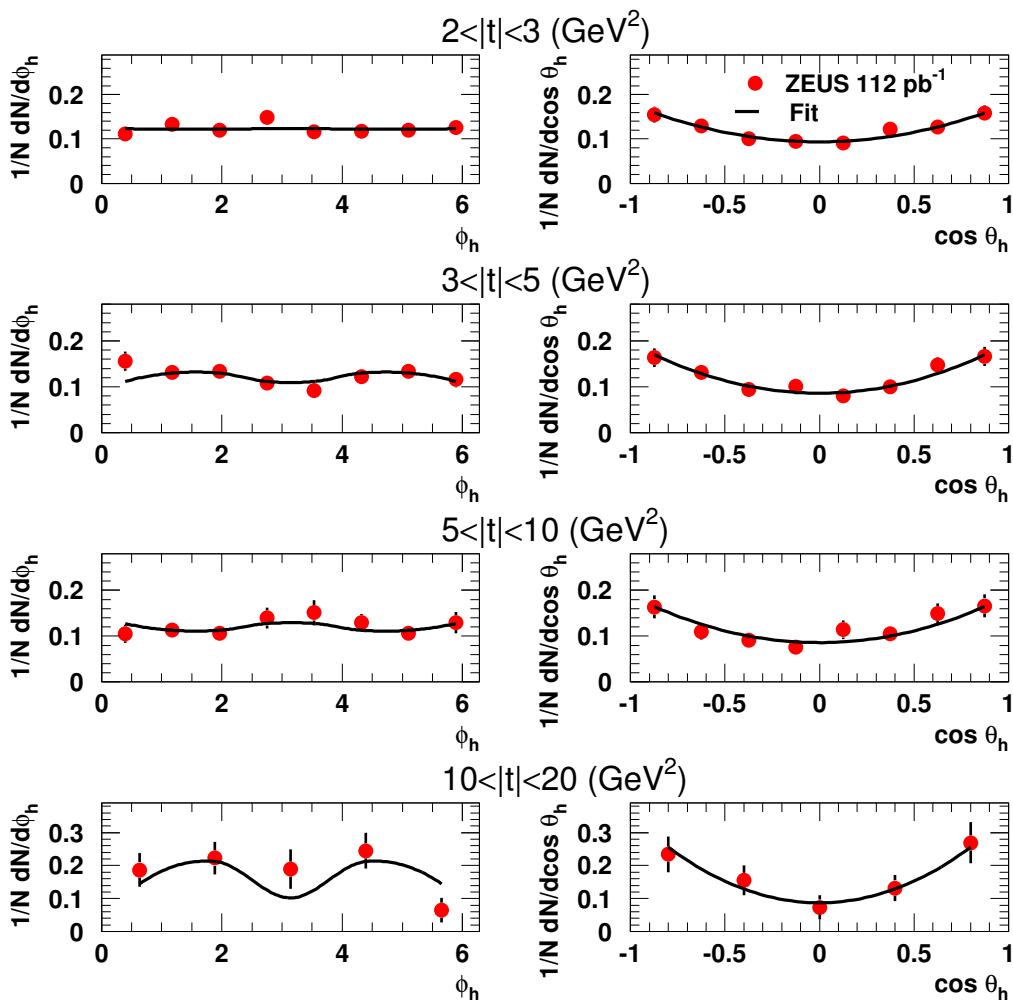
Figure 10. The normalized distributions of ϕ and $\cos(\theta)$ for $30 < W < 160\,\mathrm{GeV}$ and $z > 0.95$ in four bins of $|t|$. Error bars represent only statistical uncertainties. The lines represent the results of the fits according to formulae (8.7) and (8.8) in the text.
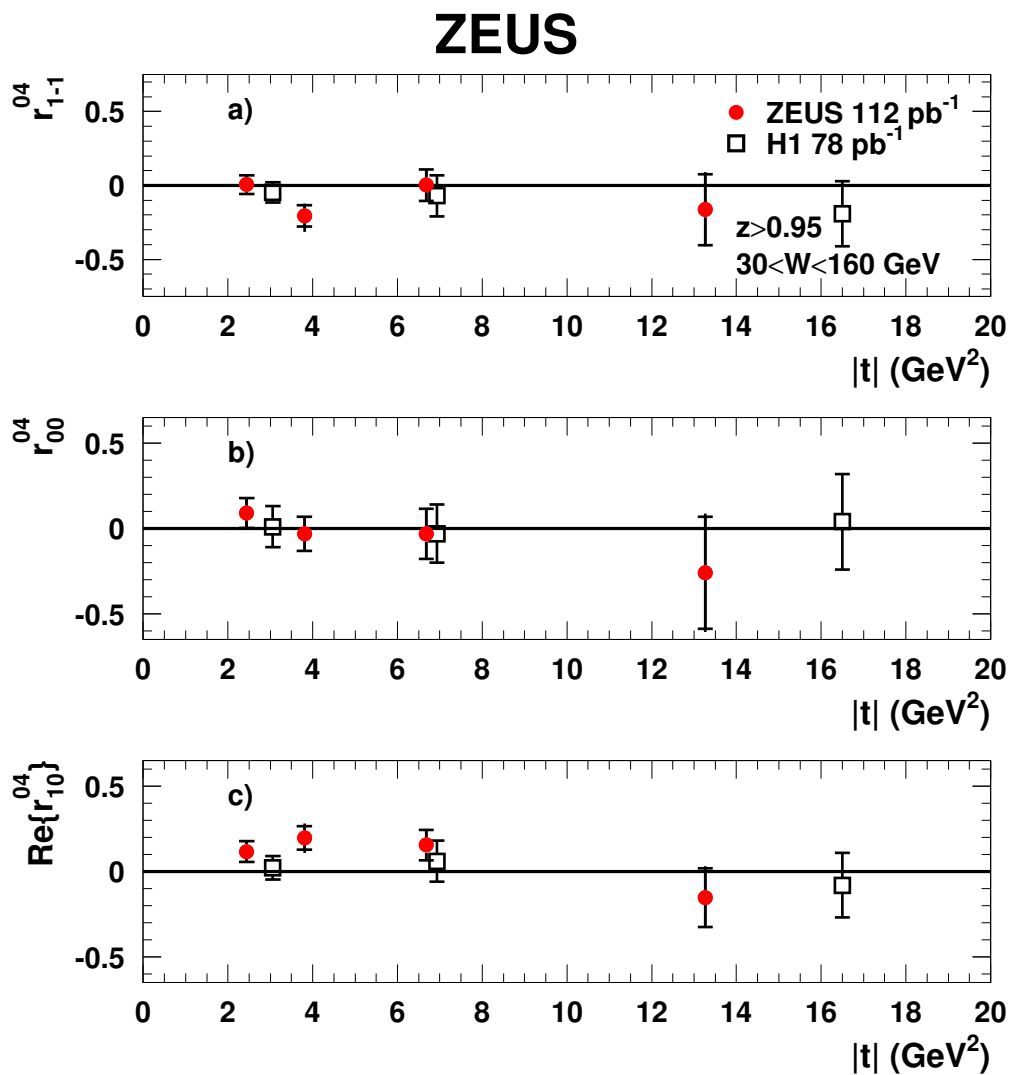
Figure 11. Helicity spin density matrix elements a) r^{04}_{1-1}, b) r^{04}_{00} and c) $\mathrm{Re}\{r^{04}_{10}\}$ as a function of $|t|$ in the range $30 < W < 160\,\mathrm{GeV}$ and $z > 0.95$. The H1 data, $50 < W < 150$, [43] are also shown. The inner bars correspond to the statistical uncertainties and the outer to the statistical and systematic uncertainties added in quadrature. The solid lines show the expectation from SCHC.

The ZEUS Collaboration

S. Chekanov, M. Derrick, S. Magill, B. Musgrave, D. Nicholass,[1] J. Repond, R. Yoshida
Argonne National Laboratory,
Argonne, Illinois 60439-4815, U.S.A.[n]

M.C.K. Mattingly
Andrews University,
Berrien Springs, Michigan 49104-0380, U.S.A.

P. Antonioli, G. Bari, L. Bellagamba, D. Boscherini, A. Bruni, G. Bruni, F. Cindolo,
M. Corradi, G. Iacobucci, A. Margotti, R. Nania, A. Polini
INFN Bologna,
Bologna, Italy[e]

S. Antonelli, M. Basile, M. Bindi, L. Cifarelli, A. Contin, S. De Pasquale,[2] G. Sartorelli,
A. Zichichi
University and INFN Bologna,
Bologna, Italy[e]

D. Bartsch, I. Brock, H. Hartmann, E. Hilger, H.-P. Jakob, M. Jüngst, A.E. Nuncio-Quiroz,
E. Paul, U. Samson, V. Schönberg, R. Shehzadi, M. Wlasenko
Physikalisches Institut der Universität Bonn,
Bonn, Germany[b]

J.D. Morris[3]
H.H. Wills Physics Laboratory, University of Bristol,
Bristol, United Kingdom[m]

M. Kaur, P. Kaur,[4] I. Singh[4]
Panjab University, Department of Physics,
Chandigarh, India

M. Capua, S. Fazio, A. Mastroberardino, M. Schioppa, G. Susinno, E. Tassi[5]
Calabria University, Physics Department and INFN,
Cosenza, Italy[e]

J.Y. Kim[6]
Chonnam National University,
Kwangju, South Korea

Z.A. Ibrahim, F. Mohamad Idris, B. Kamaluddin, W.A.T. Wan Abdullah
Jabatan Fizik, Universiti Malaya,
50603 Kuala Lumpur, Malaysia[r]

Y. Ning, Z. Ren, F. Sciulli
Nevis Laboratories, Columbia University,
Irvington on Hudson, New York 10027, U.S.A.[o]

J. Chwastowski, A. Eskreys, J. Figiel, A. Galas, K. Olkiewicz, B. Pawlik, P. Stopa,
L. Zawiejski
The Henryk Niewodniczanski Institute of Nuclear Physics, Polish Academy of Sciences,
Cracow, Poland[i]

L. Adamczyk, T. Bołd, I. Grabowska-Bołd, D. Kisielewska, J. Łukasik,[7] M. Przybycień, L. Suszycki
Faculty of Physics and Applied Computer Science,
AGH-University of Science and Technology,
Cracow, Poland[p]

A. Kotański,[8] W. Słomiński[9]
Department of Physics, Jagellonian University,
Cracow, Poland

O. Bachynska, O. Behnke, J. Behr, U. Behrens, C. Blohm, K. Borras, D. Bot, R. Ciesielski, N. Coppola, S. Fang, A. Geiser, P. Göttlicher,[10] J. Grebenyuk, I. Gregor, T. Haas, W. Hain, A. Hüttmann, F. Januschek, B. Kahle, I.I. Katkov,[11] U. Klein,[12] U. Kötz, H. Kowalski, V. Libov, M. Lisovyi, E. Lobodzinska, B. Löhr, R. Mankel,[13] I.-A. Melzer-Pellmann, S. Miglioranzi,[14] A. Montanari, T. Namsoo, D. Notz, A. Parenti, P. Roloff, I. Rubinsky, U. Schneekloth, A. Spiridonov,[15] D. Szuba,[16] J. Szuba,[17] T. Theedt, J. Tomaszewska,[18] G. Wolf, K. Wrona, A.G. Yagües-Molina, C. Youngman, W. Zeuner[13]
Deutsches Elektronen-Synchrotron DESY,
Hamburg, Germany

V. Drugakov, W. Lohmann, S. Schlenstedt
Deutsches Elektronen-Synchrotron DESY,
Zeuthen, Germany

G. Barbagli, E. Gallo
INFN Florence,
Florence, Italy[e]

P.G. Pelfer
University and INFN Florence,
Florence, Italy[e]

A. Bamberger, D. Dobur, F. Karstens, N.N. Vlasov[19]
Fakultät für Physik der Universität Freiburg i.Br.,
Freiburg i.Br., Germany[b]

P.J. Bussey, A.T. Doyle, M. Forrest, D.H. Saxon, I.O. Skillicorn
Department of Physics and Astronomy, University of Glasgow,
Glasgow, United Kingdom[m]

I. Gialas,[20] K. Papageorgiu
Department of Engineering in Management and Finance, Univ. of the Aegean,
Chios, Greece

U. Holm, R. Klanner, E. Lohrmann, H. Perrey, P. Schleper, T. Schörner-Sadenius, J. Sztuk, H. Stadie, M. Turcato
Hamburg University, Institute of Exp. Physics,
Hamburg, Germany[b]

K.R. Long, A.D. Tapper
Imperial College London, High Energy Nuclear Physics Group,
London, United Kingdom[m]

T. Matsumoto,[21] K. Nagano, K. Tokushuku,[22] S. Yamada, Y. Yamazaki[23]
Institute of Particle and Nuclear Studies, KEK,
Tsukuba, Japan[f]

A.N. Barakbaev, E.G. Boos, N.S. Pokrovskiy, B.O. Zhautykov
Institute of Physics and Technology of Ministry of Education and Science of Kazakhstan,
Almaty, Kazakhstan

V. Aushev,[24] M. Borodin, I. Kadenko, Ie. Korol, O. Kuprash, D. Lontkovskyi, I. Makarenko,
Yu. Onishchuk, A. Salii, Iu. Sorokin, A. Verbytskyi, V. Viazlo, O. Volynets, O. Zenaiev,
M. Zolko
Institute for Nuclear Research, National Academy of Sciences,
and Kiev National University,
Kiev, Ukraine

D. Son
Kyungpook National University, Center for High Energy Physics,
Daegu, South Korea[g]

J. de Favereau, K. Piotrzkowski
Institut de Physique Nucléaire, Université Catholique de Louvain,
Louvain-la-Neuve, Belgium[q]

F. Barreiro, C. Glasman, M. Jimenez, J. del Peso, E. Ron, J. Terrón, C. Uribe-Estrada
Departamento de Física Teórica, Universidad Autónoma de Madrid,
Madrid, Spain[l]

F. Corriveau, J. Schwartz, C. Zhou
Department of Physics, McGill University,
Montréal, Québec,H3A 2T8 Canada[a]

T. Tsurugai
Meiji Gakuin University, Faculty of General Education,
Yokohama, Japan[f]

A. Antonov, B.A. Dolgoshein, D. Gladkov, V. Sosnovtsev, A. Stifutkin, S. Suchkov
Moscow Engineering Physics Institute,
Moscow, Russia[j]

R.K. Dementiev, P.F. Ermolov,[†] L.K. Gladilin, Yu.A. Golubkov, L.A. Khein, I.A. Korzhavina,
V.A. Kuzmin, B.B. Levchenko,[25] O.Yu. Lukina, A.S. Proskuryakov, L.M. Shcheglova,
D.S. Zotkin
Moscow State University, Institute of Nuclear Physics,
Moscow, Russia[k]

I. Abt, A. Caldwell, D. Kollar, B. Reisert, W.B. Schmidke
Max-Planck-Institut für Physik,
München, Germany

G. Grigorescu, A. Keramidas, E. Koffeman, P. Kooijman, A. Pellegrino, H. Tiecke,
M. Vázquez,[14] L. Wiggers

NIKHEF and University of Amsterdam,
Amsterdam, Netherlands [h]

N. Brümmer, B. Bylsma, L.S. Durkin, A. Lee, T.Y. Ling

Physics Department, Ohio State University,
Columbus, Ohio 43210, U.S.A. [n]

A.M. Cooper-Sarkar, R.C.E. Devenish, J. Ferrando, B. Foster, C. Gwenlan,[26] K. Horton,[27]
K. Oliver, A. Robertson, R. Walczak

Department of Physics, University of Oxford,
Oxford, United Kingdom [m]

A. Bertolin, F. Dal Corso, S. Dusini, A. Longhin, L. Stanco

INFN Padova,
Padova, Italy [e]

R. Brugnera, R. Carlin, A. Garfagnini, S. Limentani

Dipartimento di Fisica dell' Università and INFN,
Padova, Italy [e]

A. Raval, J.J. Whitmore[28]

Department of Physics, Pennsylvania State University, University Park,
Pennsylvania 16802, U.S.A. [o]

Y. Iga

Polytechnic University,
Sagamihara, Japan [f]

G. D'Agostini, G. Marini, A. Nigro

Dipartimento di Fisica, Università 'La Sapienza' and INFN,
Rome, Italy [e]

J.C. Hart

Rutherford Appleton Laboratory,
Chilton, Didcot, Oxon, United Kingdom [m]

H. Abramowicz,[29] R. Ingbir, S. Kananov, A. Levy, A. Stern

Raymond and Beverly Sackler Faculty of Exact Sciences, School of Physics,
Tel Aviv University, Tel Aviv, Israel [d]

M. Ishitsuka, T. Kanno, M. Kuze, J. Maeda

Department of Physics, Tokyo Institute of Technology,
Tokyo, Japan [f]

R. Hori, N. Okazaki, S. Shimizu[14]

Department of Physics, University of Tokyo,
Tokyo, Japan [f]

 R. Hamatsu, S. Kitamura,[30] O. Ota,[31] Y.D. Ri[32]

Tokyo Metropolitan University, Department of Physics,
Tokyo, Japan [f]

M. Costa, M.I. Ferrero, V. Monaco, R. Sacchi, V. Sola, A. Solano

Università di Torino and INFN,

Torino, Italy [e]

M. Arneodo, M. Ruspa

Università del Piemonte Orientale,

Novara, Italy

and INFN,

Torino, Italy [e]

S. Fourletov,[33] J.F. Martin, T.P. Stewart

Department of Physics, University of Toronto,

Toronto, Ontario, M5S 1A7 Canada [a]

S.K. Boutle,[20] J.M. Butterworth, T.W. Jones, J.H. Loizides, M. Wing

Physics and Astronomy Department, University College London,

London, United Kingdom [m]

B. Brzozowska, J. Ciborowski,[34] G. Grzelak, P. Kulinski, P. Łużniak,[35] J. Malka,[35] R.J. Nowak, J.M. Pawlak, W. Perlanski,[35] A.F. Żarnecki

Warsaw University, Institute of Experimental Physics,

Warsaw, Poland

M. Adamus, P. Plucinski,[36] T. Tymieniecka[37]

Institute for Nuclear Studies,

Warsaw, Poland

Y. Eisenberg, D. Hochman, U. Karshon

Department of Particle Physics, Weizmann Institute,

Rehovot, Israel [c]

E. Brownson, D.D. Reeder, A.A. Savin, W.H. Smith, H. Wolfe

Department of Physics, University of Wisconsin,

Madison, Wisconsin 53706, U.S.A. [n]

S. Bhadra, C.D. Catterall, G. Hartner, U. Noor, J. Whyte

Department of Physics, York University,

Ontario, M3J 1P3 Canada [a]

References

[1] P.D.B. Collins, *An Introduction to Regge Theory and High Energy Physics*. Cambridge University Press, Cambridge U.K. (1977).

[2] J.J. Sakurai, *Theory of strong interactions*, *Annals Phys.* **11** (1960) 1 [SPIRES].

[3] J.J. Sakurai, *Vector meson dominance and high-energy electron proton inelastic scattering*, *Phys. Rev. Lett.* **22** (1969) 981 [SPIRES].

[4] I.P. Ivanov, N.N. Nikolaev and A.A. Savin, *Diffractive vector meson production at HERA: From soft to hard QCD*, *Phys. Part. Nucl.* **37** (2006) 1 [hep-ph/0501034].

[5] H. Abramowicz, L. Frankfurt and M. Strikman, *Interplay of hard and soft physics in small x deep inelastic processes*, *Surveys High Energy Phys.* **11** (1997) 51.

[6] J.R. Forshaw and M.G. Ryskin, *Diffractive vector meson production at large momentum transfer*, *Z. Phys.* **C 68** (1995) 137 [hep-ph/9501376] [SPIRES].

[7] J. Bartels, J.R. Forshaw, H. Lotter and M. Wusthoff, *Diffractive Production of Vector Mesons at Large t*, *Phys. Lett.* **B 375** (1996) 301 [`hep-ph/9601201`] [SPIRES].

[8] J.R. Forshaw and G. Poludniowski, *Vector meson photoproduction at high-t and comparison to HERA data*, *Eur. Phys. J.* **C 26** (2003) 411 [`hep-ph/0107068`] [SPIRES].

[9] R. Enberg, L. Motyka and G. Poludniowski, *Diffractive heavy vector meson production from the BFKL equation*, *Eur. Phys. J.* **C 26** (2002) 219 [`hep-ph/0207027`] [SPIRES].

[10] E.A. Kuraev, L.N. Lipatov and V.S. Fadin, *Multi-Reggeon Processes in the Yang-Mills Theory*, *Sov. Phys. JETP* **44** (1976) 443 [SPIRES].

[11] E.A. Kuraev, L.N. Lipatov and V.S. Fadin, *The Pomeranchuk Singularity in Nonabelian Gauge Theories*, *Sov. Phys. JETP* **45** (1977) 199 [SPIRES].

[12] I.I. Balitsky and L.N. Lipatov, *The Pomeranchuk Singularity in Quantum Chromodynamics*, *Sov. J. Nucl. Phys.* **28** (1978) 822 [SPIRES].

[13] ZEUS collaboration, S. Chekanov et al., *Measurement of proton dissociative diffractive photoproduction of vector mesons at large momentum transfer at HERA*, *Eur. Phys. J.* **C 26** (2003) 389 [`hep-ex/0205081`] [SPIRES].

[14] ZEUS collaboration, U. Holm, *The ZEUS Detector*, Status Report (unpublished), DESY (1993), available on http://www-zeus.desy.de/bluebook/bluebook.html.

[15] N. Harnew et al., *Vertex Triggering Using Time Difference Measurements in the ZEUS Central Tracking Detector*, *Nucl. Instrum. Meth.* **A 279** (1989) 290 [SPIRES].

[16] B. Foster et al., *The performance of the ZEUS central tracking detector z-by-timing electronics in a transputer based data acquisition system*, *Nucl. Phys. Proc. Suppl.* **B 32** (1993) 181.

[17] ZEUS collaboration, B. Foster et al., *The Design and construction of the ZEUS central tracking detector*, *Nucl. Instrum. Meth.* **A 338** (1994) 254 [SPIRES].

[18] M. Derrick et al., *Design and construction of the ZEUS barrel calorimeter*, *Nucl. Instrum. Meth.* **A 309** (1991) 77 [SPIRES].

[19] ZEUS CALORIMETER GROUP collaboration, A. Andresen et al., *Construction and beam test of the ZEUS forward and rear calorimeter*, *Nucl. Instrum. Meth.* **A 309** (1991) 101 [SPIRES].

[20] A. Caldwell et al., *Design and implementation of a high precision readout system for the ZEUS calorimeter*, *Nucl. Instrum. Meth.* **A 321** (1992) 356 [SPIRES].

[21] ZEUS BARREL CALORIMETER GROUP collaboration, A. Bernstein et al., *Beam tests of the ZEUS barrel calorimeter*, *Nucl. Instrum. Meth.* **A 336** (1993) 23 [SPIRES].

[22] G. Abbiendi et al., *The ZEUS barrel and rear muon detector*, *Nucl. Instrum. Meth.* **A 333** (1993) 342 [SPIRES].

[23] ZEUS LUMINOSITY GROUP collaboration, J. Andruszkow et al., *Luminosity measurement in the ZEUS experiment*, *Acta Phys. Polon.* **B 32** (2001) 2025 [SPIRES].

[24] W.H. Smith, K. Tokushuku and L.W. Wiggers, Proceedings of *Computing in High-Energy Physics (CHEP)*, Annecy France, September 1992, C. Verkerk and W. Wojcik eds., CERN, Geneva, Switzerland (1992), pg. 222, also in preprint DESY 92-150B.

[25] V.N. Gribov and L.N. Lipatov, *Deep inelastic e p scattering in perturbation theory*, *Sov. J. Nucl. Phys.* **15** (1972) 438 [SPIRES].

[26] V.N. Gribov and L.N. Lipatov, *e^+e^- pair annihilation and deep inelastic e p scattering in perturbation theory*, *Sov. J. Nucl. Phys.* **15** (1972) 675 [SPIRES].

[27] Y.L. Dokshitzer, *Calculation of the Structure Functions for Deep Inelastic Scattering and e^+e^- Annihilation by Perturbation Theory in Quantum Chromodynamics*, *Sov. Phys. JETP* **46** (1977) 641 [SPIRES].

[28] G. Altarelli and G. Parisi, *Asymptotic Freedom in Parton Language*, *Nucl. Phys.* **B 126** (1977) 298 [SPIRES].

[29] E. Gotsman, E. Levin, U. Maor and E. Naftali, *Momentum transfer dependence of the differential cross section for J/ψ production*, *Phys. Lett.* **B 532** (2002) 37 [hep-ph/0110256] [SPIRES].

[30] A.H. Mueller and W.-K. Tang, *High-energy parton-parton elastic scattering in QCD*, *Phys. Lett.* **B 284** (1992) 123 [SPIRES].

[31] R. Enberg, J.R. Forshaw, L. Motyka and G. Poludniowski, *Vector meson photoproduction from the BFKL equation. I: Theory*, *JHEP* **09** (2003) 008 [hep-ph/0306232] [SPIRES].

[32] G.G. Poludniowski, R. Enberg, J.R. Forshaw and L. Motyka, *Vector meson photoproduction from the BFKL equation. II: Phenomenology*, *JHEP* **12** (2003) 002 [hep-ph/0311017] [SPIRES].

[33] L. Frankfurt, M. Strikman and M. Zhalov, *Large t diffractive J/ψ photoproduction with proton dissociation in ultraperipheral pA collisions at LHC*, *Phys. Lett.* **B 670** (2008) 32 [arXiv:0807.2208] [SPIRES].

[34] L. Frankfurt and M. Strikman, *Large t, triple Pomeron diffractive processes in QCD*, *Phys. Rev. Lett.* **63** (1989) 1914 [SPIRES].

[35] R. Brun et al., *GEANT 3.13*, 1987 CERN DD/EE/84-1.

[36] M. Kasprzak, *Inclusive properties of diffractive and nondiffractive photoproduction at HERA*, Ph.D. Thesis, Warsaw University, Warsaw, Poland (1996), Report DESY F35D-96-16.

[37] L. Adamczyk, *Vector Meson Photoproduction at Large Momentum Transfer at HERA*, Ph.D. Thesis, University of Mining and Metallurgy, Cracow, Poland (1999), Report DESY-THESIS-1999-045.

[38] T. Abe, *GRAPE-Dilepton (Version 1.1): A generator for dilepton production in e p collisions*, *Comput. Phys. Commun.* **136** (2001) 126 [hep-ph/0012029] [SPIRES].

[39] M. Arneodo, L. Lamberti and M. Ryskin, *DIPSI: A Monte Carlo generator for elastic vector meson production in charged lepton proton scattering*, *Comput. Phys. Commun.* **100** (1997) 195 [hep-ph/9610286] [SPIRES].

[40] M. Turcato, *Open beauty photoproduction at HERA*, Ph.D. Thesis, Univeersity of Padova, Padova, Italy (2002), Report DESY-THESIS-2003-039.

[41] V. M. Budnev, I. F. Ginzburg, G. V. Meledin and V. G. Serbo, *The Two photon particle production mechanism. Physical problems. Applications. Equivalent photon approximation*, *Phys. Rept.* **15** (1975) 181 [SPIRES].

[42] J. Pumplin et al., *New generation of parton distributions with uncertainties from global QCD analysis*, *JHEP* **07** (2002) 012 [hep-ph/0201195] [SPIRES].

[43] H1 collaboration, A. Aktas et al., *Diffractive photoproduction of J/ψ mesons with large momentum transfer at HERA*, *Phys. Lett.* **B 568** (2003) 205 [hep-ex/0306013] [SPIRES].

[44] A. Donnachie and P.V. Landshoff, *Total cross-sections*, *Phys. Lett.* **B 296** (1992) 227 [hep-ph/9209205] [SPIRES].

[45] A. Donnachie and P.V. Landshoff, *pp and p̄p Elastic Scattering*, *Nucl. Phys.* **B 231** (1984) 189 [SPIRES].

[46] S.J. Brodsky, V.S. Fadin, V.T. Kim, L.N. Lipatov and G.B. Pivovarov, *The QCD Pomeron with optimal renormalization*, *JETP Lett.* **70** (1999) 155 [hep-ph/9901229] [SPIRES].

[47] N.N. Nikolaev, B.G. Zakharov and V.R. Zoller, *Exploratory study of shrinkage of the diffraction cone for the generalized BFKL Pomeron*, *Phys. Lett.* **B 366** (1996) 337 [hep-ph/9506281] [SPIRES].